SCIENTIFIC REPORTS
nature research

Check for updates

OPEN

Simple rapid stabilization method through citric acid modification for magnetite nanoparticles

Mohammed Ali Dheyab[1,2]✉, Azlan Abdul Aziz[1,2]✉, Mahmood S. Jameel[1,2], Osama Abu Noqta[1,2], Pegah Moradi Khaniabadi[1,2] & Baharak Mehrdel[1,2]

A highly stable and magnetized citric acid (CA)-functionalized iron oxide aqueous colloidal solution (Fe_3O_4@CA) was synthesized by using a simple and rapid method of one-step co-participation via a chemical reaction between Fe^{3+} and Fe^{2+} in a NaOH solution at 65 °C, followed by CA addition to functionalize the Fe_3O_4 surface in 25 min. The NPs were synthesized at lower temperatures and shortened time compared with conventional methods. Surface functionalization is highly suggested because bare Fe_3O_4 nanoparticles (Fe_3O_4 NPs) are frequently deficient due to their low stability and hydrophilicity. Hence, 19 nm-sized Fe_3O_4 NPs coated with CA (Fe_3O_4@CA) were synthesized, and their microstructure, morphology, and magnetic properties were characterized using X-ray diffraction, transmission electron microscopy, Zeta potential, Fourier transform infrared spectroscopy, and vibrating sample magnetometer. CA successfully modified the Fe_3O_4 surface to obtain a stabilized (homogeneous and well dispersed) aqueous colloidal solution. The Zeta potential value of the as-prepared Fe_3O_4@CA increases from − 31 to − 45 mV. These CA-functionalized NPs with high magnetic saturation (54.8 emu/g) show promising biomedical applications.

Fe_3O_4 NPs with a grain size of smaller than 20 nm display superparamagnetic behavior at high temperatures but exhibit no coercivity and remanence at room temperature[1–4]. These particles are extensively utilized for several biomedical and in vivo applications[5–9]. Fe_3O_4 NPs, a well-known ferrofluid, has been expansively analyzed, particularly their colloidal dispersion and many potential biomedical applications. The surface of magnetite particles is modified by different coating agents, including protein[10], methoxypoly (ethylene glycol)[11], dextran[12], chitosan[13], and silica coating[14], to enhance their performance. Controlling the sizes and dispersion of NPs in preferred solvents is technologically challenging due to difficulties faced in their fabrication and handling for biomedical applications, including their clustering/aggregation, homogeneity, hydrophilicity, and biocompatibility[15,16]. The high surface energies of NPs are attributed to their large surface to volume ratio. NPs tend to aggregate to minimize total surface energy, which exceeds 0.1 N/m for metal oxide surfaces[17].

Proper functionalization of NP surface and solvent selection are critical to attain adequate repelling interactions between the NPs to inhibit agglomeration/accretion and improve the thermodynamic stability of the colloidal solution. The surface of Fe_3O_4 dispersed in aqueous media via citric acid adsorption can be functionalized by utilizing the coordination of one or two carboxylate functionalities of the citric acid depending on the steric necessity and curvature of the surface[18]. Carboxylates significantly affect the development of Fe_3O_4 NPs and their magnetic characteristics. Surface modification of aqueous magnetic NPs by using heavy chain fatty acid or thiol is one of the methods to increase the stability of NP suspension[19]. Co-precipitation is typically used to synthesize water-stable Fe_3O_4 NPs and considered as the simplest, most cost-effective technique requiring the lowest temperature[20]. However, its main drawbacks are the agglomeration, broad size distribution, poor Zeta potential values of NPs. Fe_3O_4 NPs also lack good colloidal stability and have inadequate repulsive forces to prevent agglomeration. The poor colloidal stability and broad size distribution can be attributed to the reaction time and temperature during co-precipitation. To overcome these problems, the Fe_3O_4 NPs must be stabilized and their size distribution must be reduced by modifying their surfaces with biocompatible materials, in addition to controlling the synthesis procedures. Nevertheless, most of aqueous stabilized Fe_3O_4 NPs are achieved

[1]Nano-Biotechnology Research and Innovation (NanoBRI), Institute for Research in Molecular Medicine (INFORMM), Universiti Sains Malaysia, 11800 Pulau Pinang, Malaysia. [2]Nano-Optoelectronics Research and Technology Lab (NORLab), School of Physics, Universiti Sains Malaysia, 11800 Pulau Pinang, Malaysia. ✉email: mohammed@student.usm.my; lan@usm.my

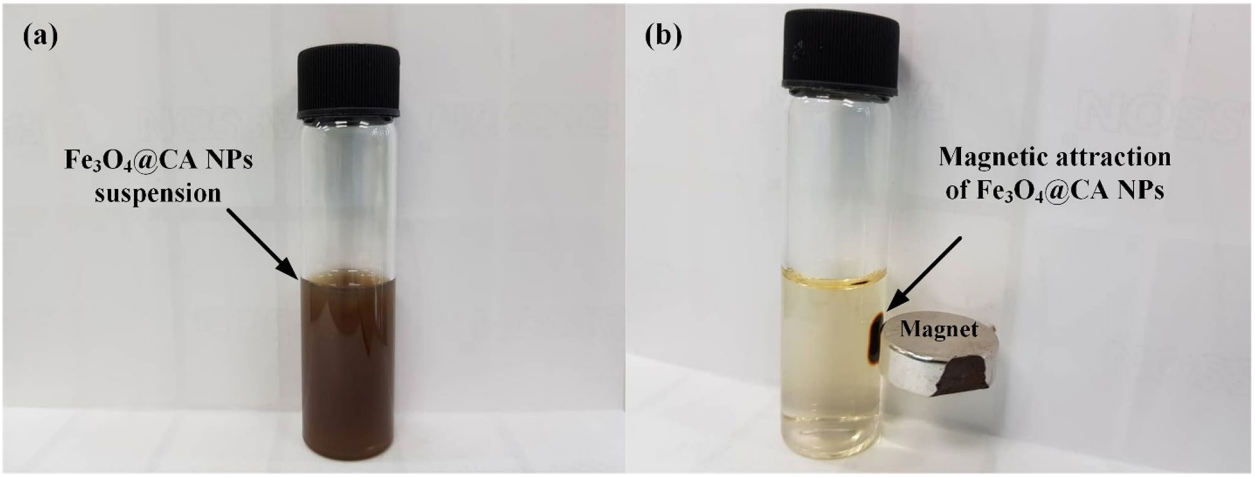

Figure 1. Magnetic attraction of Fe_3O_4@CA NPs: (**a**) Fe_3O_4@CANPs in solution state and (**b**) magnetic attraction of Fe_3O_4@CA NPs toward a magnet.

either at high temperature[21–23] or long reaction time[24–26]. For example, Elham et al.[27] and Arefi et al.[28] synthesized citric acid (CA)-stabilized Fe_3O_4 NPs through two-step co-precipitation that is laborious and time consuming. In addition, Singh et al.[29] synthesized CA-coated Fe_3O_4 NPs through co-precipitation, and the transmission electron microscopy (TEM) results indicated that the NPs have agglomerated and are non-uniform in shape.

To the extent of our knowledge, the stability of Fe_3O_4@CA NPs has not been reported. Therefore, this study aims (1) to synthesize a highly stable and magnetized Fe_3O_4@CA aqueous colloidal solution by employing a one-step, fast, and straightforward route (with shortened time and lower temperature than conventional methods) and systematically controlling and manipulating the flow of the reaction procedure and (2) to develop surface functional groups on magnetic NP derivatization through a one-step process.

Materials and methods

Materials. Ferric chloride ($FeCl_3{\cdot}6H_2O$, 99%), ferrous chloride ($FeCl_2{\cdot}4H_2O$, 99%), and sodium hydroxide (NaOH) were acquired from Sigma–Aldrich, and citric acid (CA) were purchased from Merck.

Preparation Fe_3O_4@CA. Fe_3O_4 NPs were synthesized through the co-precipitation of ferrous (Fe^{2+}) and ferric (Fe^{3+}) with sodium hydroxide (NaOH). $FeCl_2.4H_2O$ (2.5 g) and $FeCl_3.6H_2O$ (4.0 g) were dissolved in 180 mL of distilled water under nitrogen gas. Following the complete dissolution of the mixture at room temperature, 50 mL of sodium hydroxide was drop-wise added to the reaction mixture, which was mechanically stirred at 650 rpm and kept for 10 min at 65 °C under continuous vigorous stirring. For the prevention of Fe_3O_4 NP agglomeration, 150 mL of CA was added to the reaction mixture, which was then stirred for 10 min (65 °C). Fe_3O_4@CA NPs were collected through a permanent magnet and thoroughly rinsed four times with distilled water to eliminate unreactive or inert impurities. Finally, the Fe_3O_4@CA NPs were redispersed in the distilled water after sonication for 5 min, and the resulting suspension (Fe_3O_4@CA) responded to an external magnetic field as shown in Fig. 1.

Characterization of Fe_3O_4@CA. X-ray diffraction (XRD) patterns were obtained using an X-ray diffractometer (PANalytical X'pert PRO MRD PW 3040) with CuKa ($\lambda = 1.54050$ Å). The size of Fe_3O_4 NPs and Fe_3O_4@Au CSNPs were obtained by transmission electron microscopic (TEM) using a Zeiss Libra 120 at 100 kV. Particle size distribution was measured using ImageJ software. The stability (Zeta potential) of Fe_3O_4@CA NPs was described using a dynamic light scattering (DLS) instrument (ZETASIZER Nanoseries Model ZEN 3600, Malvern Instruments). The surface functional groups of Fe_3O_4@CA NPs were determined by Fourier transform infrared spectroscopy (PERKIN ELMER System 2000 FT-IR). Magnetic properties were evaluated using vibrating sample magnetometer (VSM, DMS MODEL 8810).

Results and discussion

Fe_3O_4 NP surfaces were functionalized via CA adsorption, which occurs by coordinating one or two of the carboxylate functionalities depending on the need for steric repelling to stabilize the ferrofluids and the curvature or morphology of the surface. Nonetheless, a minimum of one carboxylic acid group is exposed to the solvent, thus accounting for the surface charging. The presence of a carboxylic group surface ligand offers the possibility of developing bonds with proteins, fluorescent dyes, and hormone linkers to facilitate precise targeting in biological systems. The one-step modification of the superparamagnetic Fe_3O_4 NP surface is presented in Fig. 2, and the as-prepared Fe_3O_4 NPs were subsequently stabilized with CA to prevent agglomeration.

The XRD spectra (Fig. 3) of Fe_3O_4 NPs confirmed their cubic spinel structure with high crystallinity. These diffraction peaks are narrow and well defined, indicating the high crystallinity of the sample. The positions and intensities of the diffraction peaks for NPs are consistent those of Fe_3O_4 (Ref. Code 01-075-0033). The synthesis

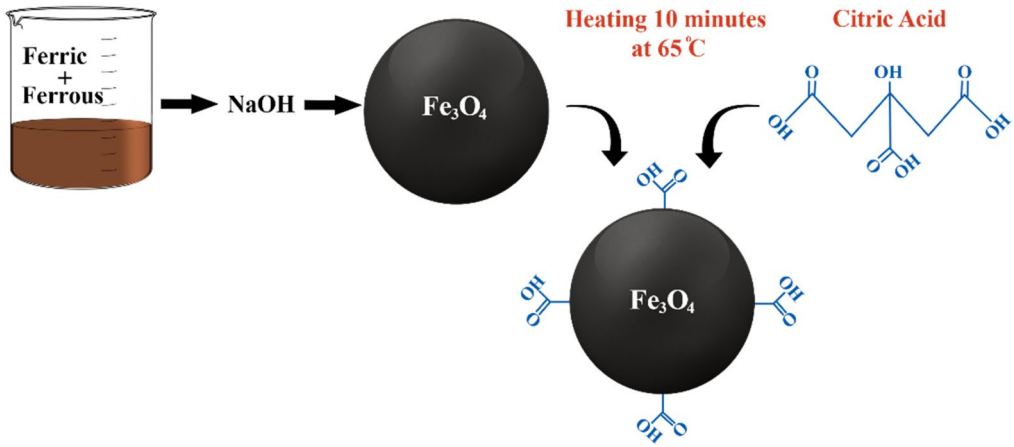

Figure 2. Steps for CA functionalization of Fe_3O_4 NP surface in 25 min.

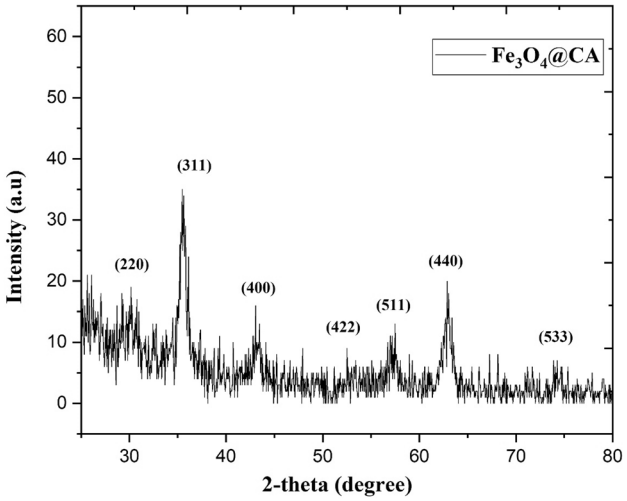

Figure 3. XRD spectra of the CA-functionalized Fe_3O_4 NPs showing the composition and crystal structure of Fe_3O_4.

method for Fe_3O_4 particles via the co-precipitation of Fe^{2+} and Fe^{3+} in an aqueous base solution is a relatively established and extensively utilized procedure[25,30]. The XRD results are consistent with the possible constituents of Fe_3O_4 particles. The diffraction peaks denote the crystallinity of Fe_3O_4 NPs as spinel cubic lattice type. Nevertheless, further oxidation of the Fe_2O_3 phase was not verified by the XRD data due to the similarity between lattice type and constant[31]. According to a previous study, the CA coating for Fe_3O_4 NPs does not result in the phase change in the XRD spectra of bare Fe_3O_4[29].

The TEM image and size distribution of the as-synthesized Fe_3O_4 and Fe_3O_4@CA NPs are presented in (Fig. 4). Figure 4a shows the TEM image of Fe_3O_4 prior to CA modification. A slightly important change in Fe_3O_4 agglomeration was induced by CA. From the histogram in Fig. 4c, the average size of the monodispersed Fe_3O_4@CA NPs is approximately 19 nm. The Fe_3O_4@CA NPs are spherical in shape with a narrow size distribution after CA modification, particularly at stable synthesis conditions. The TEM images of the CA-functionalized superparamagnetic Fe_3O_4 NPs show semi-spherical shaped particles and monodispersion. Previous studies used co-precipitation to synthesize CA-coated Fe_3O_4 and produced agglomerated NPs with average sizes 51[28], 50[32], 25,[33] and 22 nm[34], which might be due to the high reaction temperature[35].

Figure 5 presents the stability of Fe_3O_4 after CA modification to show the role of CA on the stability of Fe_3O_4 NPs. The Zeta potential magnitude of Fe_3O_4 NPs was measured immediately after the synthesis of the particles, followed by CA injection on the colloidal Fe_3O_4 NPs. Dispersion stability can be defined in relation to the Zeta potential value (mV): 0 to ± 5 can cause the rapid agglomeration and precipitation of NP suspension, ± 10 to ± 30 is responsible for the threshold of delicate dispersion, ± 30 to ± 40 denotes the moderate stability of colloidal NPs[36–39], and ± 40 to ± 60 indicates the excellent stability of NP suspension referred to as a high charge on their surface[40]. The measured results indicate that Zeta potential improves from − 31.3 to − 45.3 mV (Fig. 5a, b), which is higher than the reported values[41–43] and is attributed to the three carboxylate groups of citrate that dissociate

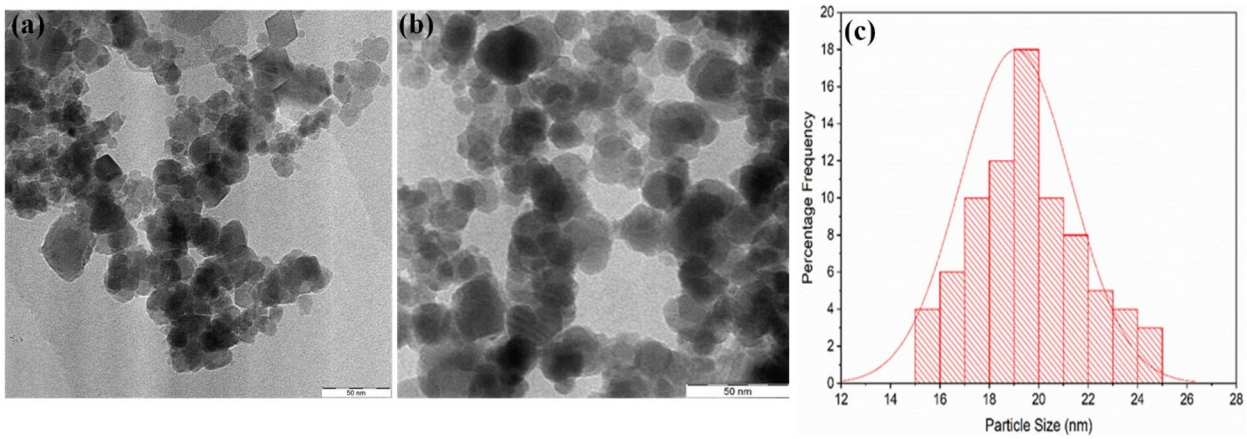

Figure 4. TEM micrographs of (**a**) bare Fe_3O_4, (**b**) Fe_3O_4@CA, and (**c**) the corresponding size distribution of Fe_3O_4@CA.

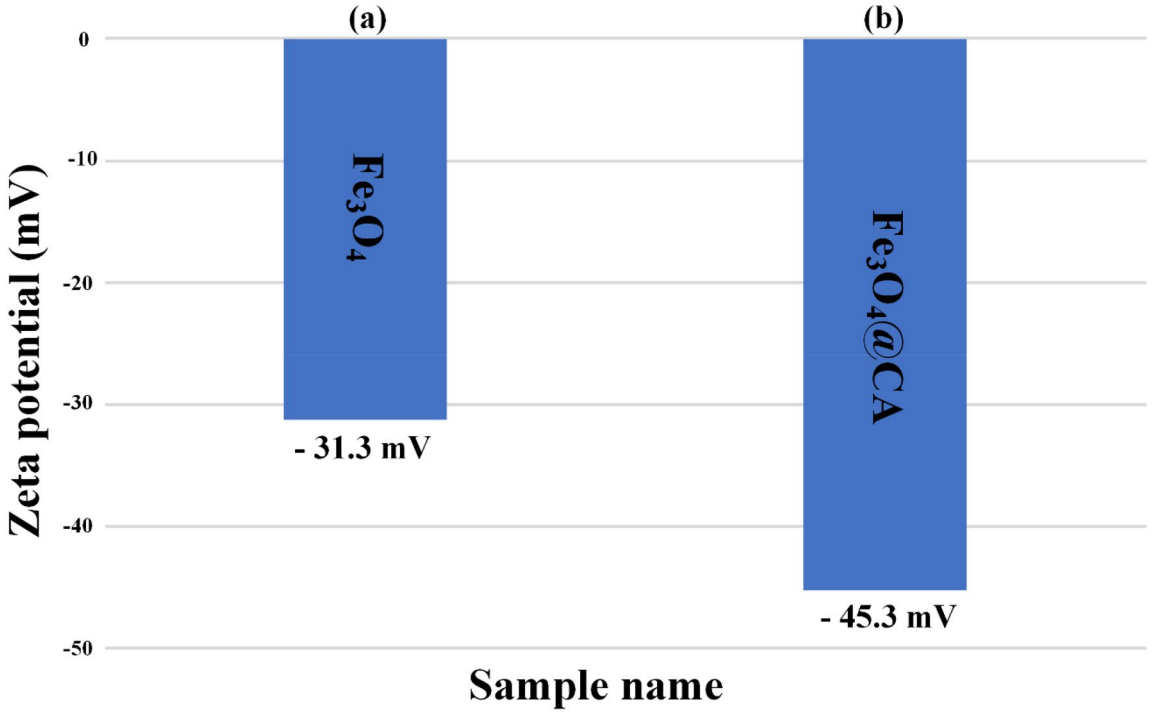

Figure 5. Stability measurement of as-synthesized nanoparticles using Zeta potential for (**a**) bare Fe_3O_4 and (**b**) Fe_3O_4@CA.

and strongly bind with Fe_3O_4 NP surface[18]. In addition, the negative charge of the Zeta potential is due to the electrostatic stabilization provided by the strong adsorption of citrate ions on NP surface. The Zeta potential of CA-coated Fe_3O_4 has not been reported. The increase in the measured Zeta potential revealed that CA is absorbed onto the Fe_3O_4 NP surface, thus resulting in a highly negative surface charge. The presence of carboxylate group is confirmed by monitoring the Zeta potential for Fe_3O_4 NPs. However, this study characterized and analyzed only the results for a moderately polydispersed sample.

The Fourier transform-infrared spectroscopy (FT-IR) spectrum of bare Fe_3O_4 has been reported[28,29]. This study aimed to prove the presence of CA on the Fe_3O_4 surface. FT-IR spectra of CA and Fe_3O_4@CA NPs are illustrated in Fig. 6a and b. The spectrum peak was assigned to the CA-coated Fe_3O_4 NPs. The broad band spectrum at 3,384 cm^{-1} can be referred to as the OH band groups and to the traces of molecular water. The 1722 cm^{-1} spectrum peak of CA is due to the symmetric C=O stretching from the COOH group. This peak display shifts to a lower wavelength at approximately 1615 cm^{-1} for the carboxylic group (R-OOH) of the Fe_3O_4@CA. The peak

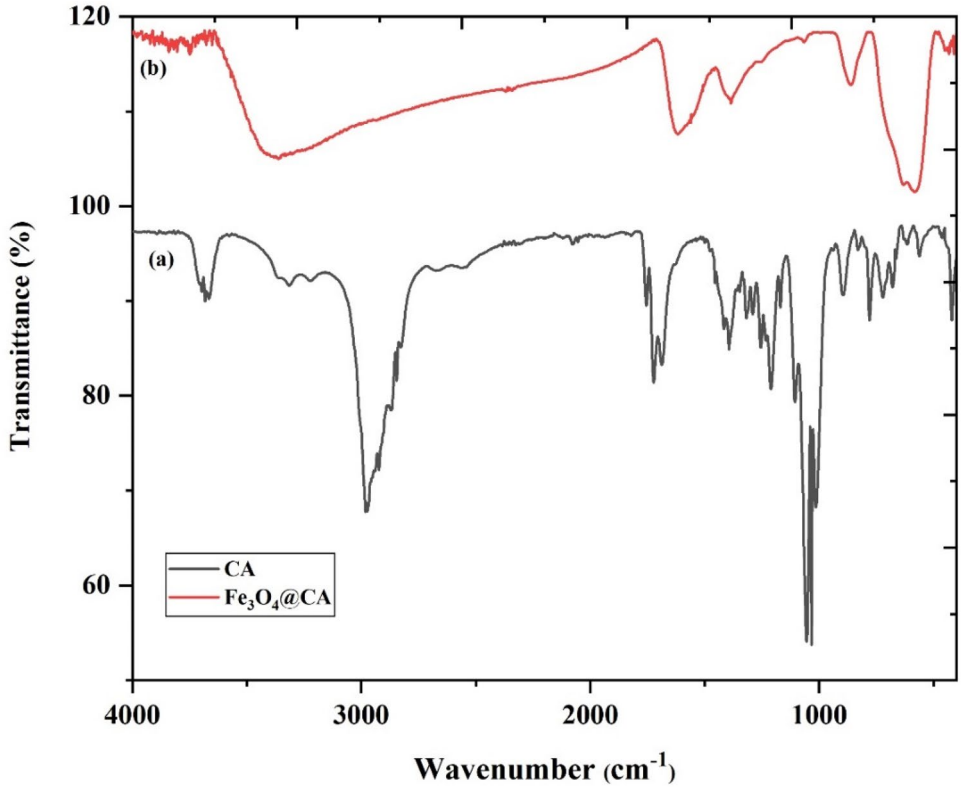

Figure 6. FTIR spectra of (**a**) bare CA and (**b**) CA conjugated on the surface of Fe_3O_4 NPs.

at 1615 cm^{-1} determines the binding of CA radical on the surface of Fe_3O_4 NPs through the chemisorption of carboxylate citrate ions[28,29]. The peak at 1,384 cm^{-1} can be ascribed to the asymmetric stretching of C–O from the carboxylic group. The intense peak observed at the IR range at approximately 578 cm^{-1} in Fe_3O_4@CA could be assigned to the Fe–O stretching vibrational mode of Fe_3O_4[44]. Hence, CA binds to the Fe_3O_4 surface through carboxylate.

The magnetic properties of Fe_3O_4@CA were determined by VSM analysis at room temperature. The magnetization saturation (emu/g) as a function of the applied magnetic field (Oe) is illustrated in Fig. 7. The magnetization curve shows that the Fe_3O_4@CA NPs exhibit a superparamagnetic behavior and magnetic saturation (Ms) of approximately 54.8 emu/g, which is higher than that in previous studies[25,33] (Table 1) possibly due to the low Fe oxidation state. No hysteresis was observed, and the behavior was completely reversible at 300 K. Neither coercivity nor remanence was observed. Arefi et al.[28]. reported that the Ms of bare Fe_3O_4 is reduced after being coated with CA. Alonso et al.[23] synthesized Fe_3O_4 NPs with high crystallinity of approximately 35 nm and high Ms of 65 emu/g by using thermal decomposition. The high Ms value is attributed to the large particle size of Fe_3O_4[45]. Therefore, the Ms of Fe_3O_4 NPs decreases with their reduced particle size due to the increase in surface spin disorder[46,47]. In this case, the size reduction to the nanoscale (below 20 nm) for spherical single-component Fe_3O_4 greatly influences the magnetic ordering of surface spins, namely, a high degree of disordered surface spins of Fe_3O_4 NPs. Spherical Fe_3O_4 NPs could develop surface spin disorder through energy minimization. The disordered surface spins are highly anisotropic, which is in line with the increase in their effective magnetic anisotropy.

For biomedical applications such as in hyperthermia and magnetic resonance imaging (MRI), NPs must have a uniform particle size, exhibit superparamagnetism, and possess high Ms. The as-synthesized Fe_3O_4@CA has a high magnetic response, which is preferable for biomedical applications[28]. Our method shows an advantage of having a simple and rapid route to synthesize highly stable (− 45.3 mV), monodispersed, and superparamagnetic Fe_3O_4@CA (19 nm) compared with conventional techniques.

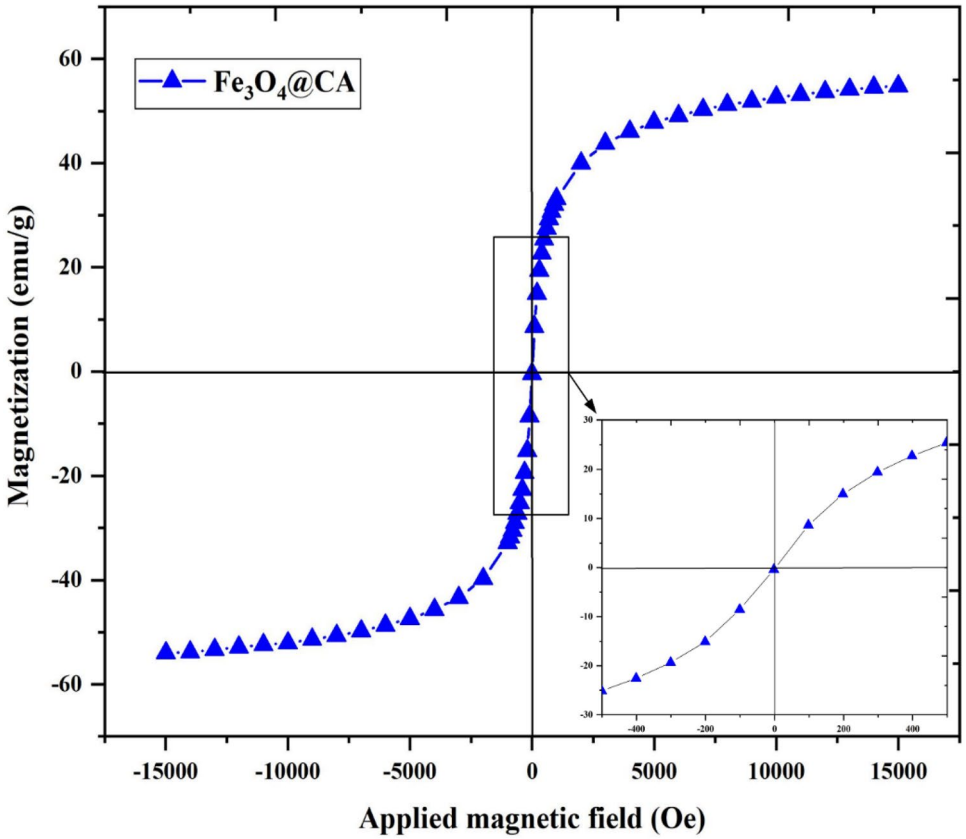

Figure 7. Magnetization curve of superparamagnetic (no coercivity or remanence) Fe_3O_4@CA at room temperature.

No.	Method	Reaction Time (minutes)	Temperature °C	Saturation magnetization (emu/g)	Ref.
1	Co-precipitation	60	90	46	[33]
2	Co-precipitation	120	–	32.40	[25]
3	Co-precipitation	150	90	74	[27]
4	Co-precipitation	120	–	55	[28]
5	Co-precipitation	35	90	–	[29]
6	Present study	25	65	54.8	

Table 1. Comparison with previous studies on Fe_3O_4 synthesis.

Conclusion

We developed a simple and rapid synthesis route for highly stable and superparamagnetic Fe_3O_4@CA through co-precipitation. The proposed method requires simple equipment and cheap materials such as a magnetic stirrer, and the processing time was 25 min at 65 °C. The NPs were achieved at lower temperature, simpler process, and shorter time compared with conventional methods. XRD, TEM, Zeta potential, FT-IR, and VSM were employed to characterize the microstructure and morphology of the synthesized NPs. The presence of carboxylate group is confirmed by FTIR analysis, and the Zeta potential for Fe_3O_4 particles was monitored. The Zeta potential value of as-prepared Fe_3O_4@CA increased from – 31.3 to – 45.3 mV. Finally, these NPs are important for several biomedical applications due to their small size, stability, and superparamagnetic behavior.

Received: 27 October 2019; Accepted: 16 June 2020
Published online: 01 July 2020

References

1. Ángeles-Pascual, A. *et al.* Structure, magnetic and cytotoxic behaviour of solvothermally grown Fe3O4@ Au core-shell nanoparticles. *Mater. Charact.* **142**, 237–244 (2018).

2. Khaniabadi, P. M. *et al.* Magnetic iron oxide nanoparticles as T2 MR imaging contrast agent for detection of breast cancer (MCF-7) cell. *Avicenna J Med Biotechnol* **9**, 181 (2017).
3. Dheyab, M. A., Aziz, A. A., Jameel, M. S., Khaniabadi, P. M. & Mehrdel, B. Mechanisms of effective gold shell on Fe_3O_4 core nanoparticles formation using sonochemistry method. *Ultrason. Sonochem.* **104**, 865 (2019).
4. 4Dheyab, M. *et al.* in *Journal of Physics: Conference Series*. 012003.
5. Lai, W.-Y. *et al.* In vivo investigation into effectiveness of Fe_3O_4/PLLA nanofibers for bone tissue engineering applications. *Polymers* **10**, 804 (2018).
6. Wang, K. *et al.* Fe3O4@ astragalus polysaccharide core-shell nanoparticles for iron deficiency anemia therapy and magnetic resonance imaging in vivo. *ACS Appl. Mater. Interfaces.* **11**, 10452–10461 (2019).
7. Rajkumar, S. & Prabaharan, M. *Noble Metal-Metal Oxide Hybrid Nanoparticles* 607–623 (Elsevier, Amsterdam, 2019).
8. Khaniabadi, P. M., Shahbazi-Gahrouei, D., Majid, A. M. S. A. & Khaniabadi, B. M. Study the Anti-MUC1 antibody-based iron oxide nanoparticles on three-dimension spheroid and breast cancer (MCF-7) cell imaging. *Pol. J. Med. Phys. Eng.* **25**, 69–77 (2019).
9. Khaniabadi, P. M. *et al.* In vitro study of SPIONs-C595 as molecular imaging probe for specific breast cancer (MCF-7) cells detection. *Ir. Biomed. J.* **21**, 360 (2017).
10. 10Zorin, V. *et al. Journal of Physics: Conference Series*. 031009 (IOP Publishing).
11. PolymersAli, S. *et al.* Synthesis, characterization, and relaxometry studies of hydrophilic and hydrophobic superparamagnetic Fe_3O_4 nanoparticles for oil reservoir applications. *Colloids Surf. A* **543**, 133–143 (2018).
12. Patil, R. M. & Shete, P. B. *Biodistribution Interaction Nanostructures of Hybrid* (Elesiver, Amsterdam, 2018).
13. Ge, J., Zhai, M., Zhang, Y., Bian, J. & Wu, J. Biocompatible Fe_3O_4/chitosan scaffolds with high magnetism. *Int. J. Biol. Macromol.* **128**, 406–413 (2019).
14. Iqbal, M. Z. *et al.* A facile fabrication route for binary transition metal oxide-based janus nanoparticles for cancer theranostic applications. *Nano Res.* **11**, 5735–5750 (2018).
15. Liu, J. *et al.* Highly water-dispersible biocompatible magnetite particles with low cytotoxicity stabilized by citrate groups. *Angew. Chem. Int. Ed.* **48**, 5875–5879 (2009).
16. Nigam, S., Barick, K. & Bahadur, D. Development of citrate-stabilized Fe_3O_4 nanoparticles: conjugation and release of doxorubicin for therapeutic applications. *J. Magn. Magn. Mater.* **323**, 237–243 (2011).
17. Gavilán, H., Brollo, M., Gutiérrez, L., Veintemillas-Verdaguer, S. & Morales, M. *Controlling the Size and Shape of Uniform Magnetic Iron Oxide Nanoparticles for Biomedical Applications* (CRC Press, Boca Raton, 2018).
18. Sahoo, Y. *et al.* Aqueous ferrofluid of magnetite nanoparticles: fluorescence labeling and magnetophoretic control. *J. Phys. Chem. B* **109**, 3879–3885 (2005).
19. Shen, L., Stachowiak, A., Fateen, S.-E.K., Laibinis, P. E. & Hatton, T. A. Structure of alkanoic acid stabilized magnetic fluids. A small-angle neutron and light scattering analysis. *Langmuir* **17**, 288–299 (2001).
20. Dheyab, M. A., Aziz, A. A., Jameel, M. S., Noqta, O. A. & Mehrdel, B. Synthesis and coating methods of biocompatible iron oxide/gold nanoparticle and nanocomposite for biomedical applications. *Chin. J. Phys.* **36**, 305–325 (2019).
21. Eom, Y., Abbas, M., Noh, H. & Kim, C. Morphology-controlled synthesis of highly crystalline Fe_3O_4 and $CoFe_2O_4$ nanoparticles using a facile thermal decomposition method. *RSC Adv.* **6**, 15861–15867 (2016).
22. Smith, M., McKeague, M. & DeRosa, M. C. Synthesis, transfer, and characterization of core-shell gold-coated magnetic nanoparticles. *MethodsX* **6**, 333–354 (2019).
23. Nemati, Z. *et al.* Enhanced magnetic hyperthermia in iron oxide nano-octopods: size and anisotropy effects. *J. Phys. Chem. C* **120**, 8370–8379 (2016).
24. Kataria, N. & Garg, V. Green synthesis of Fe_3O_4 nanoparticles loaded sawdust carbon for cadmium (II) removal from water: regeneration and mechanism. *Chemosphere* **208**, 818–828 (2018).
25. Kalantari, K. *et al.* Size-controlled synthesis of Fe_3O_4 magnetic nanoparticles in the layers of montmorillonite. *J. Nanomater.* **2014**, 181 (2014).
26. Das, R. *et al.* Tunable high aspect ratio iron oxide nanorods for enhanced hyperthermia. *J. Phys. Chem. C* **120**, 10086–10093 (2016).
27. Cheraghipour, E., Javadpour, S. & Mehdizadeh, A. R. Citrate capped superparamagnetic iron oxide nanoparticles used for hyperthermia therapy. *J. Biomed. Sci. Eng.* **5**, 715 (2012).
28. Arefi, M., Miraki, M. K., Mostafalu, R., Satari, M. & Heydari, A. Citric acid stabilized on the surface of magnetic nanoparticles as an efficient and recyclable catalyst for transamidation of carboxamides, phthalimide, urea and thiourea with amines under neat conditions. *J. Iran. Chem. Soc.* **16**, 393–400 (2019).
29. Singh, D. *et al.* Citric acid coated magnetic nanoparticles: synthesis, characterization and application in removal of Cd(II) ions from aqueous solution. *J. Water Process Eng.* **4**, 233–241 (2014).
30. Zhou, H. *et al.* Ultrasensitive DNA monitoring by Au–Fe_3O_4 nanocomplex. *Sens. Actuators B* **163**, 224–232 (2012).
31. Levy, L., Sahoo, Y., Kim, K.-S., Bergey, E. J. & Prasad, P. N. Nanochemistry: synthesis and characterization of multifunctional nanoclinics for biological applications. *Chem. Mater.* **14**, 3715–3721 (2002).
32. Patel, U., Chauhan, K. & Gupte, S. Synthesis, characterization and application of lipase-conjugated citric acid-coated magnetic nanoparticles for ester synthesis using waste frying oil. *3 Biotech* **8**, 211 (2018).
33. Li, L. *et al.* Effect of synthesis conditions on the properties of citric-acid coated iron oxide nanoparticles. *Microelectron. Eng.* **110**, 329–334 (2013).
34. Singha, D. *et al.* Citric acid coated magnetic nanoparticles: synthesis, characterization and application in removal of Cd(II) ions from aqueous solution. *J. Water Process Eng.* **4**, 233–241 (2014).
35. Zheng, B. *et al.* Plant-mediated synthesis of platinum nanoparticles and its bioreductive mechanism. *J. Colloid Interface Sci.* **396**, 138–145 (2013).
36. Jameel, M. S., Aziz, A. A. & Dheyab, M. A. Comparative analysis of platinum nanoparticles synthesized using sonochemical-assisted and conventional green methods. *Nano-Struct. Nano-Obj.* **23**, 100484. https://doi.org/10.1016/j.nanoso.2020.100484 (2020).
37. Dheyab, M. A., Owaid, M. N., Rabeea, M. A., Aziz, A. A. & Jameel, M. S. Mycosynthesis of gold nanoparticles by the Portabello mushroom extract, Agaricaceae, and their efficacy for decolorization of Azo dye. *Environ. Nanotechnol. Monit. Manage.* https://doi.org/10.1016/j.enmm.2020.100312 (2020).
38. Rabeea, M. A., Owaid, M. N., Aziz, A. A., Jameel, M. S. & Dheyab, M. A. Mycosynthesis of gold nanoparticles using the extract of Flammulina velutipes, Physalacriaceae, and their efficacy for decolorization of methylene blue. *J. Environ. Chem. Eng.* **103**, 841 (2020).
39. Owaid, M. N., Rabeea, M. A., Aziz, A. A., Jameel, M. S. & Dheyab, M. A. Mushroom-assisted synthesis of triangle gold nanoparticles using the aqueous extract of fresh *Lentinula edodes* (shiitake), Omphalotaceae. *Environ. Nanotechnol. Monit. Manage.* **12**, 100270 (2019).
40. Riddick, T. M. *Control of Colloid Stability Through zeta Potential* (Livingston, Wynnewood, PA, 1968).
41. Rehana, D., Haleel, A. K. & Rahiman, A. K. Hydroxy, carboxylic and amino acid functionalized superparamagnetic iron oxide nanoparticles: synthesis, characterization and in vitro anti-cancer studies. *J. Chem. Sci.* **127**, 1155–1166 (2015).
42. Bini, R. A., Marques, R. F. C., Santos, F. J., Chaker, J. A. & Jafelicci, M. Jr. Synthesis and functionalization of magnetite nanoparticles with different amino-functional alkoxysilanes. *J. Magn. Magn. Mater.* **324**, 534–539 (2012).
43. 43Catalano, E. & Di Benedetto, A. *Journal of Physics: Conference Series*. 012010 (IOP Publishing).

44. Yamaura, M. *et al.* Preparation and characterization of (3-aminopropyl) triethoxysilane-coated magnetite nanoparticles. *J. Magn. Magn. Mater.* **279**, 210–217 (2004).
45. Jayakumar, T., Thomas, P. A. & Geraldine, P. Protective effect of an extract of the oyster mushroom, *Pleurotus ostreatus*, on antioxidants of major organs of aged rats. *Exp. Gerontol.* **42**, 183–191 (2007).
46. Bakoglidis, K., Simeonidis, K., Sakellari, D., Stefanou, G. & Angelakeris, M. Size-dependent mechanisms in AC magnetic hyperthermia response of iron-oxide nanoparticles. *IEEE Trans. Magn.* **48**, 1320–1323 (2012).
47. Phan, M.-H. *et al.* Exchange bias effects in iron oxide-based nanoparticle systems. *Nanomaterials* **6**, 221 (2016).

Acknowledgements
This work was supported by the Malaysia Ministry of Education FRGS funding [USM Grant Number 203/PFIZIK/6711768], and the authors also acknowledge the School of Physics, Universiti Sains Malaysia for providing the facilities for this research work.

Author contributions
M.A.D., A.A.A. and M.S.J. conceived the idea and designed the experiments. A.A.A. supervised all the experiments and analyses. M.A.D., M.S.J. and O.A.N. prepared materials, performed characterizations, measurements and analyzed the results. A.A.A., P.M.K. and B.M. commented on manuscript writing. M.A.D. wrote the manuscript and all authors discussed the results and commented on the manuscript of the work.

Competing interests
The authors declare no competing interests.

Additional information
Supplementary information is available for this paper at https://doi.org/10.1038/s41598-020-67869-8.

Correspondence and requests for materials should be addressed to M.A.D. or A.A.A.

Reprints and permissions information is available at www.nature.com/reprints.

Publisher's note Springer Nature remains neutral with regard to jurisdictional claims in published maps and institutional affiliations.